Hindawi
Advances in Materials Science and Engineering
Volume 2019, Article ID 8039734, 11 pages
https://doi.org/10.1155/2019/8039734

Research Article

Nondestructive Testing on Ancient Wooden Components Based on Shapley Value

Li-hong Chang,[1] **Xiao-hong Chang**,[2] **Hao Chang**,[3] **Wei Qian**,[4] **Li-ting Cheng**,[5] **and Xiao-li Han**[5]

[1]*College of Urban and Rural Development, Beijing University of Agriculture, Beijing 102206, China*
[2]*Business School, Beijing WuZi University, Beijing 101149, China*
[3]*School of Mechanical and Precision Instrument Engineering, Xi'an University of Technology, Xi'an 710048, China*
[4]*College of Architecture and Urban Planning, Beijing University of Technology, Beijing 100124, China*
[5]*College of Architecture and Civil Engineering, Beijing University of Technology, Beijing 100124, China*

Correspondence should be addressed to Li-hong Chang; changlhong@126.com

Received 25 August 2018; Revised 24 November 2018; Accepted 23 December 2018; Published 6 February 2019

Academic Editor: Lijing Wang

In this study, we propose nondestructive testing methods and combined forecasting models-based stress wave and impedance measurements to obtain accurate internal defects information for wooden building components. Internal defects data for major wooden components of an ancient building in China and reverse laboratory test data on matching tree species indicated various degrees of damage on the pavilion wood structure surface and internal defects in certain pillars. The stress wave method enabled rapid acquisition of two-dimensional plots of test sections; however, the results revealed that the area of stress wave detection was greater than the actual defect area. Moreover, the impedance meter was able to determine the defect position and type in a single path, and the actual defect area was proportional to the absolute error of the drilling resistance. By distributing the errors from the two nondestructive testing methods on the basis of a Shapley value algorithm, we determined the weights of stress wave and impedance meter data in the forecasting models and established combined forecasting models that showed greater accuracy with a mean relative error of less than 6%. This method can improve the prediction accuracy of internal defects in ancient buildings and provide effective data support for practical engineering repair and reinforcement schemes.

1. Introduction

Due to thousands of years of history, many ancient buildings in China have been registered on the World Cultural Heritage list for their unique structures and cultural, historic, and artistic value. Most principal load-bearing components of these ancient buildings are made of wood, which, in combination with tenon and mortise connectors and bracket systems, has the advantage of long service periods, earthquake resistance, and hazard mitigation. However, as a biological material, wood is anisotropic [1], and its damage features and variations differ from those of other building materials. Wooden components are affected by temperature, humidity, the environment, and service life; thus, they are vulnerable to internal deterioration such as cavities, xylophage insects, and decay [2]. This will affect their mechanical properties of strength and stiffness and even lead to collapse [3], resulting in irrecoverable losses for nonrenewable architectural heritage. Currently, internal defects in wooden components are differentiated by qualitative visual identification and simple percussion methods, which, despite being simple and practical, largely depend on experience, although testing equipment is sometimes used for assistance [4]. However, visual inspection is not effective for locating internal defects as it only involves the surface of elements. For instance, after dismantling wooden components, major errors are always found between predicted and actual internal defects. Additionally, blind dismantling of components destroys their authenticity, which not only has a serious impact on building appearance but also leads to incalculable losses. Furthermore,

this method is problematic for internal defect estimation and scientific renovation programs.

In contrast, nondestructive testing technology aims to have no effect on the appearance, internal structure, or usability of ancient wooden components; thus, it represents a significant improvement from conventional timber and wooden material testing methods [5, 6]. In recent years, by employing methods such as X-ray scanning, Pilodyn [7], vibration methods [8], stress waves, drilling resistance [9–13], and ultrasonic waves [14–16] for the nondestructive testing of internal defects, researchers have determined that stress wave and impedance meter testing methods are the most suitable for defect detection because of their convenience, security, and effective visualization of results. For example, stress wave nondestructive testing and laboratory tests of the USS Constitution ship [17] showed that when the internal material is free of defects, the propagation path between the sensors is a straight line and the wave velocity is relatively small. Conversely, the propagation path between the sensors is disturbed by defects, resulting in a curved path and clearly increased stress wave propagation velocity in rotten wooden components; thus, internal decay and degradation can be better detected by stress wave testing. In addition, tests on the wooden components of ceilings and other parts of Papa Baroque conducted by Hungarian scholars, e.g. [18], demonstrated that stress wave technology can forecast the flexural strength of a single wooden component. Chinese researchers conducted impedance meter tests on buildings including the Forbidden City and Shanhaiguan Temple and found that resistance testing values are closely related to the air-dried density; therefore, internal defects can be directly determined from the resistance curve. Nonetheless, differences exist between testing results due to the respective advantages and limitations of these two methods. Moreover, no previous research has attempted error reduction or quantified the prediction outcomes when applying these nondestructive testing methods to the internal defects of wooden components. Therefore, in order to protect original wooden structures, combined predictions should be made of the internal defects and test results should be quantified to reduce error values. Reinforcement or replacement of wooden components is a problem which needs urgent solution in ancient architecture examination, design, and renovation [19–21].

In this study, we employ stress wave and drilling resistance tests to conduct nondestructive detection testing on the wooden components of an ancient building. We then match equivalent tree species to perform reverse laboratory tests, where we simulate common internal cavity defects in ancient architecture and then establish a nondestructive combined forecasting model to improve testing accuracy. By quantifying the internal defects, we develop a novel and practical combined prediction method for the nondestructive testing of internal defects in wooden components. Therefore, this research provides strong data support for future renovation and reinforcement of wooden components, thereby promoting the conservation and effective utilization of architectural heritage.

2. Ancient Architecture Case Study

Located in the southern part of Beijing, China, the pavilion building analyzed in this study was built during the Ming Dynasty and is known as the altar. There are not many records regarding the renovation of this ancient building, and it was not renovated in recent years. In order to combat aging and damage at various levels, this building requires testing that does not damage its authenticity and involves minimal intervention.

According to the "*Technical Code for Maintenance and Strengthening of Ancient Timber Buildings*" (national standard of the People's Republic of China GB 50165-92), the ratio of the area of decay and aging metamorphism to the area of the whole section is p. Moreover, $p > 1/5$ is regarded as damage through decay and aging of the surface layer of the bearing timber pillar, $p > 1/7$ is considered as damage due to decay of the core material, and $p > 1/8$ is considered as residual damage through decay and aging of the surface layer of the beam or both ends of the beam or core.

Currently, aging and damage exists in the wooden components of the pavilion at various levels, the most prominent of which are surface damage and pollution and damage to the building materials.

2.1. Surface Damages. At the joints of the upper eaves and around the domes, the paint decorations on the rafters and sheathings have fallen off and the sheathings have rotten due to rain erosion (Figures 1(a) and 1(b)). There is also cracking and bulging and peeling of paint decorations on the partially wooden pillar plaster (Figure 1(c)), wooden components of the fence in the west of the building are seriously aged and even cracked (Figure 1(d)), and the end of the Ang, a type of wooden component, is rotten (Figure 1(e)).

2.2. Pollution and Building Material Damage. The color of the sharp wooden components at the wooden member top has changed due to mold from microorganisms in the airless atmosphere (Figure 2(a)). Additionally, during a site investigation, birds' nests were found and most wooden components were covered by their excrement and decayed (Figure 2(b)). On the upper side of the ring beams at the east side of the pavilion, the wooden components are incomplete and some are moldy (Figure 2(c)). After the site investigation, we found different degrees of damage outside the wooden components of the altar; this along with mold will lead to the degradation of components and the formation of internal damage. Therefore, the external damage affects the internal damage. In order to determine the bearing capacity and safety of wooden members, a quantification of their internal defects is required.

3. Materials and Methods

Nondestructive testing was conducted on the main wooden components of beams and pillars, and internal defect data were collected. Some of the beams and pillars were then chosen as samples for detecting the tree species of the

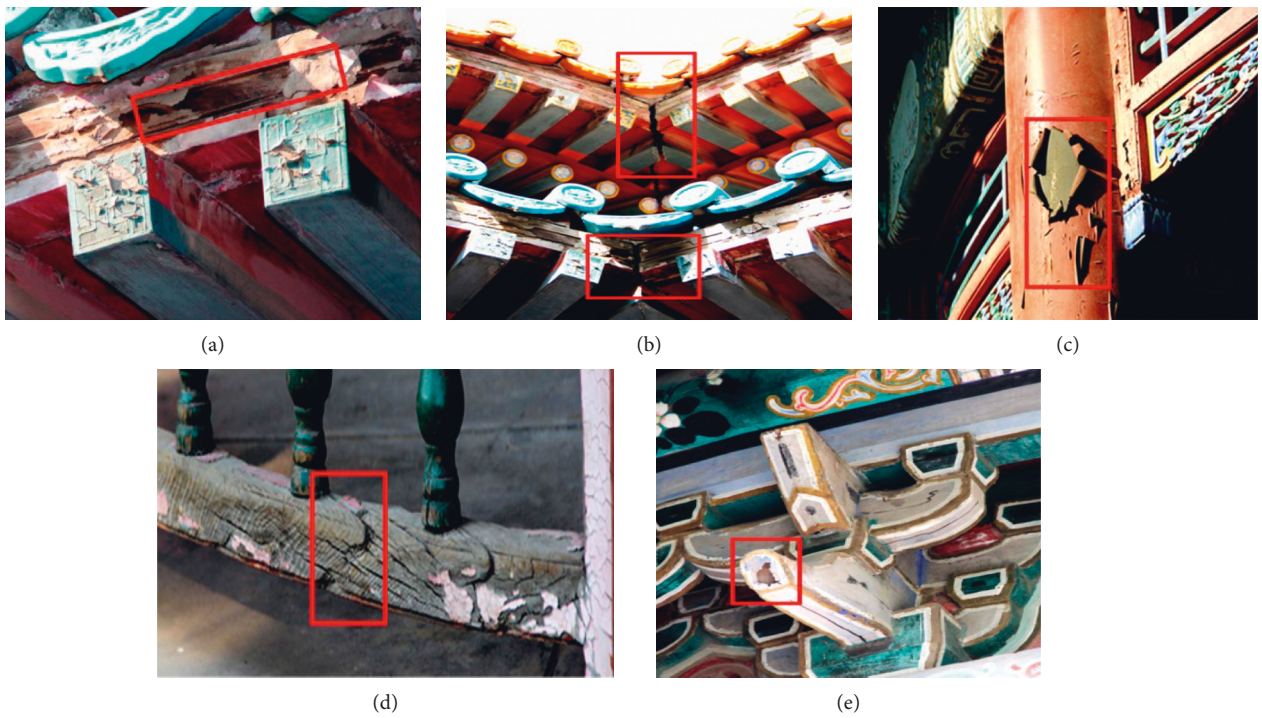

(a) (b) (c) (d) (e)

Figure 1: Surface damages of the pavilion: (a, b) eaves; (c) a pillar; (d) a fence; (e) the Ang.

(a) (b) (c)

Figure 2: Wooden component damage at the top of the pavilion due to (a, c) mold and (b) bird excrement.

components. We then matched equivalent tree species for an internal defect reverse laboratory test and analyzed the error values of each nondestructive method as well as their combined predicted values using the Shapley value algorithm. Thus, both nondestructive methods and prediction models were used to evaluate internal defect prediction of the wooden components.

3.1. Samples for Data Collection. Before that approximately ancient wooden buildings in the south and north of China were investigated (for example Shanxi Guanyin hall, Anhui Diao Xue Tang), revealing that the beam and pillar components are often damaged at both ends. Wooden pillars are eroded by rain and snow all year round, and the accumulated humidity at the bottom of the pillar, together with the normal load, encourages internal defects. The beams subject to the load of the upper wooden components all year round are easy to bend, and the overlap between beams is complex. Therefore, we focused on the internal defects of these two major wooden components. On the premise of "minimum intervention," nondestructive testing was conducted on the load-bearing beams and pillars.

3.2. Stress Wave Measurement. Internal nondestructive testing of the main load-bearing pillars and beams was conducted using the FAKOPP ten-probe stress wave measuring instrument. Stress wave sensors were installed in the top part (Section A), middle part (Section B), bottom part (Section C), beam end, and midspan (Figure 3), and testing sections were added if serious internal defects or uncertain factors were observed. Due to plaster on the pillar surfaces, the stress wave probes should be inserted to a depth of much

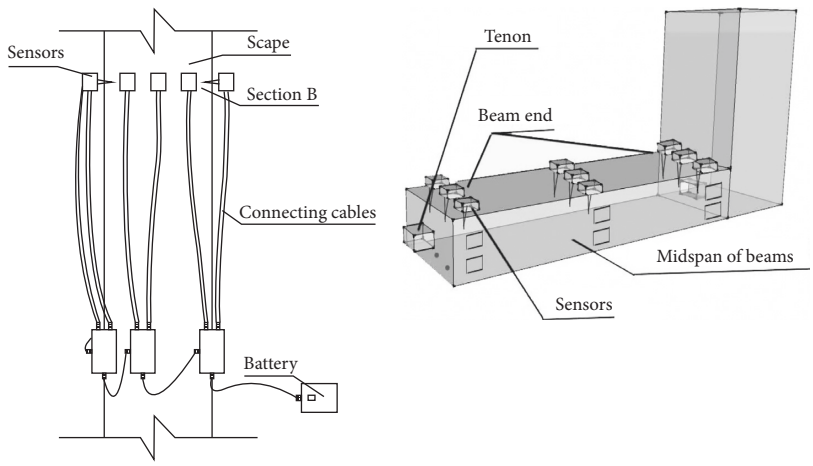

Figure 3: Stress wave sensor locations in (a) pillars and (b) beams.

greater than 50 mm for effective data collection. Sensor no. 1 was placed in the north direction, and the other sensors were distributed counterclockwise according to the perimeters of the components. The sensors were hit three consecutive times, and the average value of the resulting stress wave that propagated through the interior of the wooden components was taken as the propagation velocity. By matrix calculation and reconstruction of the propagation time of internal sections in different paths, the data were transformed into two-dimensional plots, in which the axes represent the specimen size and the left-hand color bar represents the condition of the wooden component. Dark green represents a healthy interior, which changes to yellow then red and finally blue as its condition deteriorates, representing a severe cavity. Internal defects in the wood were then analyzed using ArborSonic 3D.

3.3. Drilling Resistance Tests Method. The German-made IML-500 drill was used to conduct nondestructive drilling resistance testing on the wooden components. A microprobe with a length of 1.5 mm was driven into the interior of the components. The probe encounters different resistances as it moves forward, producing a relative resistance value of the path. This was plotted in two-dimensional plots of the internal defects where the x-axis represents the microprobe path length and the y-axis the relative resistance value (probe insertion resistance value and rotation resistance value). Based on the stress wave detection map, the defect locations of different sections were analyzed by the probe along three different paths at an angle of 60° to collect impedance meter data.

4. Results and Discussion

4.1. Tree Species Identification. Figure 4(a) and 4(b) shows pillar B2 pillar and the beam between pillars B3 and B4. Through visual observation and smell, analysis of the macroscopic texture, color, and smell characteristics shows that heartwood (pillar B2) and sapwood (beam between B3 and B4) are clearly different and have no distinct taste. Analysis of vertical sections, cross sections, and tangential sections (Figures 4(c) and 4(d)), using microscope observations of specimens at 75x magnification, indicates that the tracheids range in tangential diameter from 25 to 56 μm (average 40 μm). The transverse section of earlywood tracheids is typically oblong and rarely polygonal, and dentate ray tracheids do not exhibit thickening and are sinuous and undular [22]. Based on the macro and micro characteristics of the samples, we conclude that the samples between pillar B2 and B3-B4 are all Pinaceae Lindl, and the tree species are *Larix* of the *Larix* genus. The probe is inserted into the object to be measured by using the water content meter. After the special number is stabilized, the displayed number is the moisture value of the object to be measured. The moisture contents of the beam and pillar are less than 12%.

4.2. Wooden Components' Internal Defects Analysis. Our analysis of the internal defects of the major wooden beam and pillar components shows no defects in the interior of beam components but serious defects in the interior of pillars B2 and D4. For example, Figure 5 shows Sections A, B, and C of pillar B2. Analysis by ArborSonic 3D revealed severe internal defects in Section C and no internal defects in Sections A and B (Figure 5(a)). To estimate whether the internal defects of Section C develop upwards or become more serious, all sensors were moved upwards by 50 cm (Section D) from Section C. The results show that a clear reduction of internal defects and of the affected area (Figure 5(a)), indicating that the bottom of the pillar is the original source of defects and Section C is the main location of internal defects (Table 1). By connecting each section of pillar B2 and analyzing the entire pillar, we verify that points 2–6 of Section C are the most serious and there are no defects in the interior of Sections A and B (Figure 5(b)).

As well as using the stress wave chart to determine internal defects in Section C, targeted drilling resistance test results also reveal the locations and sizes of internal defects along a single path (Figure 6). Different internal defect

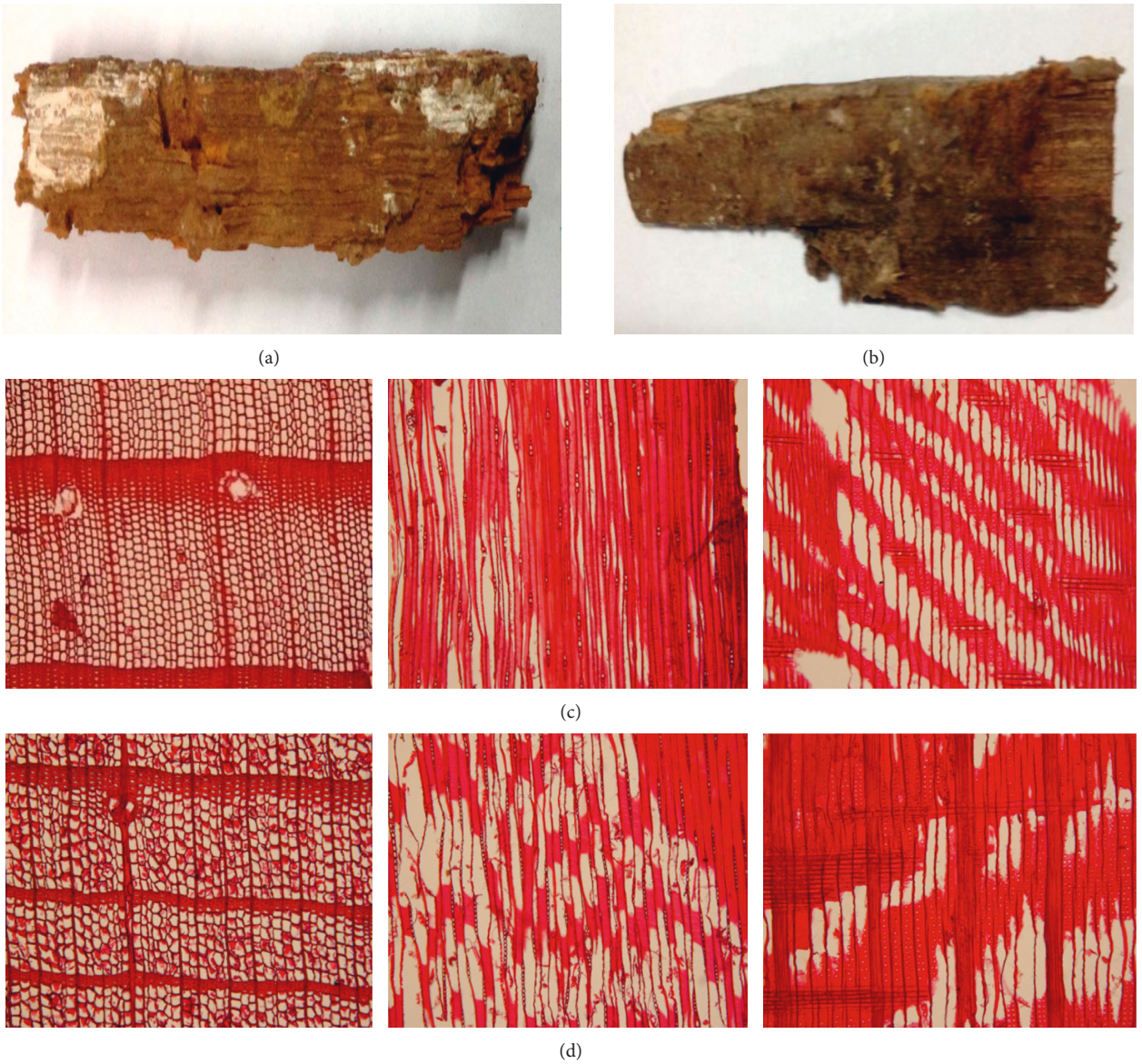

Figure 4: Analysis of wooden component samples for tree species analysis: (a) pillar B2, (b) beam between B3 and B4, (c) and (d) microscopic images of three types of section of the *Larix* tree species.

lengths (x_i, $x_{i+1}, \ldots x_n$) can be formed by intersecting the three paths, and n triangles with diverse areas can be obtained by connecting neighboring defect points. The internal defect area of the entire testing section is obtained by

$$S_2 = \sum_{i=1}^{n-1} x_i \cdot x_{i+1} \cdot \sin \frac{360^\circ}{n}, \quad (1)$$

where S_2 represents the total area of internal defects in the section, n is the number of defect edges, and x_i is the defect length. According to previous research, when relative resistance values are less than 30% or below the average wave crest of the relative resistance values in the normal range, internal defects in this range are determined as cavities or cracks. In general, cavities are longer than cracks, so the internal defects of the wooden components can be defined as internal cavities. Specific testing data are shown in Table 1.

4.3. Reverse Laboratory Test. Based on the internal defect results of the wood components in the ancient buildings, we matched equivalent tree species and then processed samples by manual digging and cutting them to size. To reduce the error value between the experimental results and the data collected from the ancient buildings, we simulated all defect types of the samples as internal holes. According to the defect locations in the wood components, the defect distribution in the specimen was simulated in the core materials and in the sapwood. The specific design parameters of specimens are shown in Table 2.

After production, the specimens were kept in the laboratory at a temperature of 20° and relative air humidity of 65% for 3 months. Tests were conducted when the air-dried moisture content was below 12%. Defect expansion over six different stages (when the defect area occupies 0, 1/9, 1/7, 1/5, 1/3, and 1/2 of the section area) demonstrates the initial,

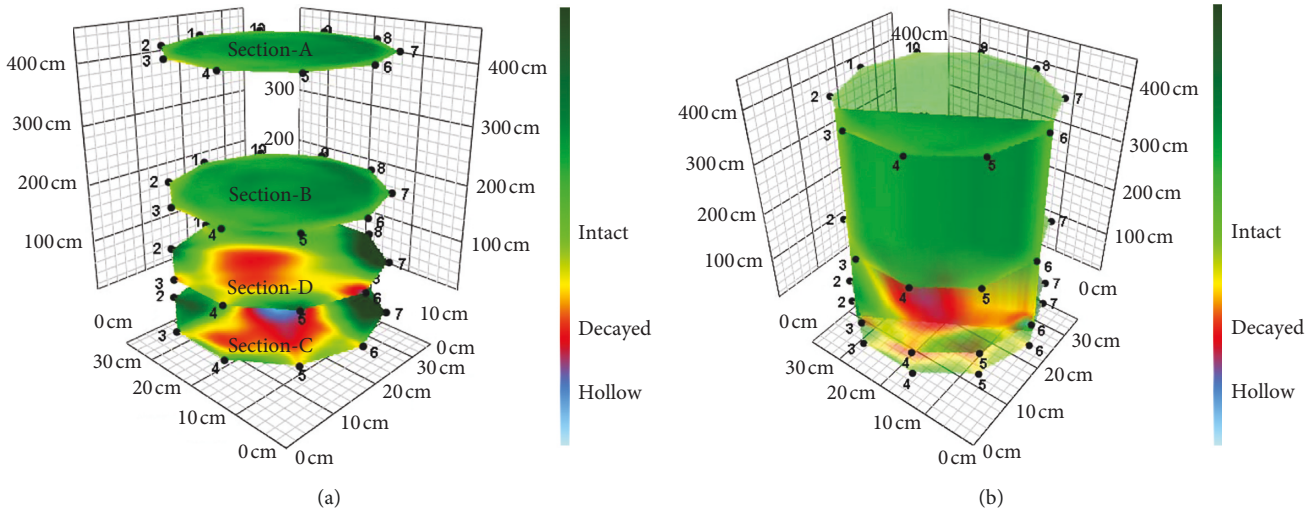

Figure 5: Stress wave analysis of pillar B2 showing (a) different sections of the pillar and (b) a longitudinal sectional of the internal defects.

Table 1: Nondestructive testing data of pillar B2.

Section names	Height (cm)	Moisture content (%)	Section area (cm^2)	Stress wave testing defect area (cm^2)	Impedance meter testing defect area (cm^2)
Section A	433.00	10	946.30	0	0
Section B	216.50	10	963.82	0	0
Section C	10.00	10	981.51	294.45	213.47
Section D	60.00	10	981.51	333.71	246.85

intermediate, and terminal stages of the defects. The average value of three hits on each sensor was taken as the propagation velocity. In order to avoid the discreteness of testing data due to specimens displaying diverse defect areas, stress wave data were collected three times. We analyzed 36 groups of nondestructive testing data and the average values of sections with the same defect areas.

Internal cavity simulation experiments of specimens D-1 and D-2 by the FAKOPP stress wave timer and IML impedance meter indicate that the larger the internal defect area, the more accurate the size and location of internal defect detection by the stress waves (Table 3). The boundaries of the cavities are blurred in the stress wave diagrams (Figures 7(a) and 7(b)). Moreover, the stress wave testing area, S_1, is larger than the specimen's actual internal defect area, S_0; the absolute error of the stress wave, R_1, is calculated as follows:

$$R_1 = |S_1 - S_0|. \quad (2)$$

R_1 and the relative error value, Q_1, vary irregularly (Table 3). This illustrates that because of the severe damage to wooden components' internal fibers, the stress wave travel path changes and the propagation time increases, which leads to errors in internal defect area detection.

The crest (maximum drilling resistance) and trough (lowest rate drilling resistance) of the relative resistance values are revealed by inserting needles during impedance meter testing; therefore, the internal defects can be defined as cavities. These cavities can be used to determine the internal defect boundary and length; however, an impedance meter only reflects the internal defects in single path, so entire section defects cannot be detected. The impedance meter testing values, S_2, of specimens are listed in Table 3. The 36 groups of experiments prove that when the internal defect is a cavity with a diameter of more than 6 cm, the probe path will change direction due to a drop in the resistance value. Moreover, unstable swinging can easily cause the probe to break off or deviate from the anticipated testing path; thus, the absolute error value of drilling resistance, R_2, is calculated as

$$R_2 = |S_2 - S_0|. \quad (3)$$

The data in Table 3 show that the R_2 value increases with defect expansion. A comparison of the above two testing methods indicates that the stress wave nondestructive testing method can make rapid and direct judgments of internal defect locations and lengths, but defect types cannot be determined clearly and defect boundaries are vague. Conversely, the impedance meter nondestructive testing method can make a precise judgment on internal defect length in a single path and quantify defect types; however, it cannot effectively determine the entire testing section, and the absolute error increases with the size of the internal cavity.

5. Numerical Analysis and Prediction Model

As shown in Table 3, errors exist in the stress wave and impedance meter nondestructive testing results, in order to reduce the area of internal defects of wood components;

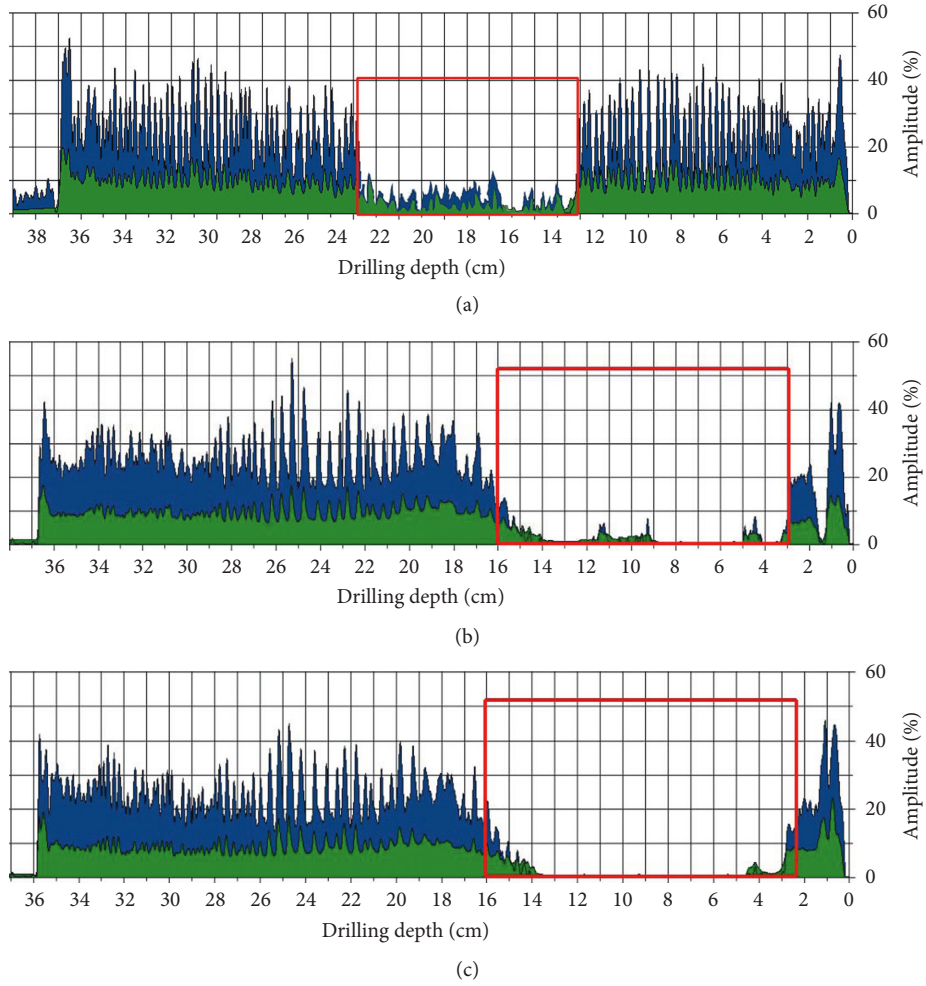

Figure 6: Two-dimensional plot of the drilling resistance results of Section C. (a) Path one. (b) Path two. (c) Path three. Note: horizontal coordinates indicate the depth of the probe path and vertical coordinates show that the density distribution and the early and late wood performance of the probe differ as the probe advances inside the pillar. Location of damaged section in red box.

Table 2: Wooden component sample descriptions used for the reverse tests.

Specimen numbers	Tree species	Perimeter (mm)	Height (mm)	Moisture content (%)	Simulation type	Testing height (mm)
D-1	*Larix*	850	100	9.4	Core material cavity	50
D-2	*Larix*	850	100	8.7	Sapwood cavity	50

therefore, we performed a combined prediction and evaluation for these two methods.

5.1. Combined Models Construction. Stress wave and impedance meter methods have both advantages and disadvantages for testing internal defect locations and areas, so their results are evaluated comprehensively in order to construct a combined prediction model. On the assumption that the same wooden component internal defects are predicted by N testing methods, the combined forecasting model of the internal defects of N testing results is

$$f_t = \sum_{i=1}^{N} K_i f_{it}, \quad (4)$$

where f_t is the predicted value of wooden component internal defects according to the combined forecasting model, f_{it} is the predicted value of i wooden component internal defects, where $i = 1,2\ldots, n$, K is the weighting of internal defects, and K_i is the weight of i wooden component internal defects, where $i = 1,2\ldots, n$ and $\sum_{i=1}^{N} K_i = 1$.

5.2. Optimal Weighting Method Based on the Shapley Value Algorithm. The combined predicted overall values of the two nondestructive testing methods are distributed by a weighting method based on the Shapley value algorithm to determine the weight of each testing value [23–25]. On the assumption that there are n nondestructive testing methods in the combined prediction, $I = \{1,2,\ldots n\}$ and, for any subset p, q

Table 3: Comparison of nondestructive testing methods.

Number	Type	Proportion	Actual defect S_0 (cm^2)	Stress wave S_1 (cm^2)	Drilling resistance S_2 (cm^2)	Combined prediction S_3 (cm^2)	Absolute error value		Relative error value		
							Stress wave R_1 (cm^2)	Drilling resistance R_2 (cm^2)	Stress wave Q_1 (%)	Impedance meter Q_2 (%)	Combined prediction Q_3 (%)
D-1	Core material cavity	0	0	0	0	0	0	0	0	0	0
		1/9	63.96	86.35	52.85	65.92	22.39	11.11	35.01	17.37	3.06
		1/7	82.24	138.16	68.11	95.43	55.92	14.13	68.00	17.18	16.04
		1/5	115.13	149.67	95.41	116.57	34.54	19.72	30.00	17.13	1.25
		1/3	191.89	178.45	158.88	178.21	16.56	33.01	8.63	17.20	7.13
		1/2	287.83	316.61	237.94	268.62	28.78	49.89	10.00	17.33	6.67
Average			123.51	144.87	102.20	120.79	26.37	21.31	25.27	14.37	5.69
D-2	Sapwood cavity	0	0	0	0	0	0	0	0	0	0
		1/9	63.96	72.08	50.73	60.34	8.12	13.23	12.70	20.69	5.66
		1/7	82.24	104.35	71.42	86.24	22.11	10.82	26.89	13.16	4.86
		1/5	115.13	155.43	92.26	120.69	40.30	22.87	35.00	19.87	4.83
		1/3	191.89	236.02	163.39	196.07	44.13	28.50	23.00	14.85	2.18
		1/2	287.83	324.29	226.54	270.53	36.46	61.29	12.67	21.29	6.01
Average			123.51	148.70	100.72	122.31	30.22	27.34	18.38	14.98	3.92

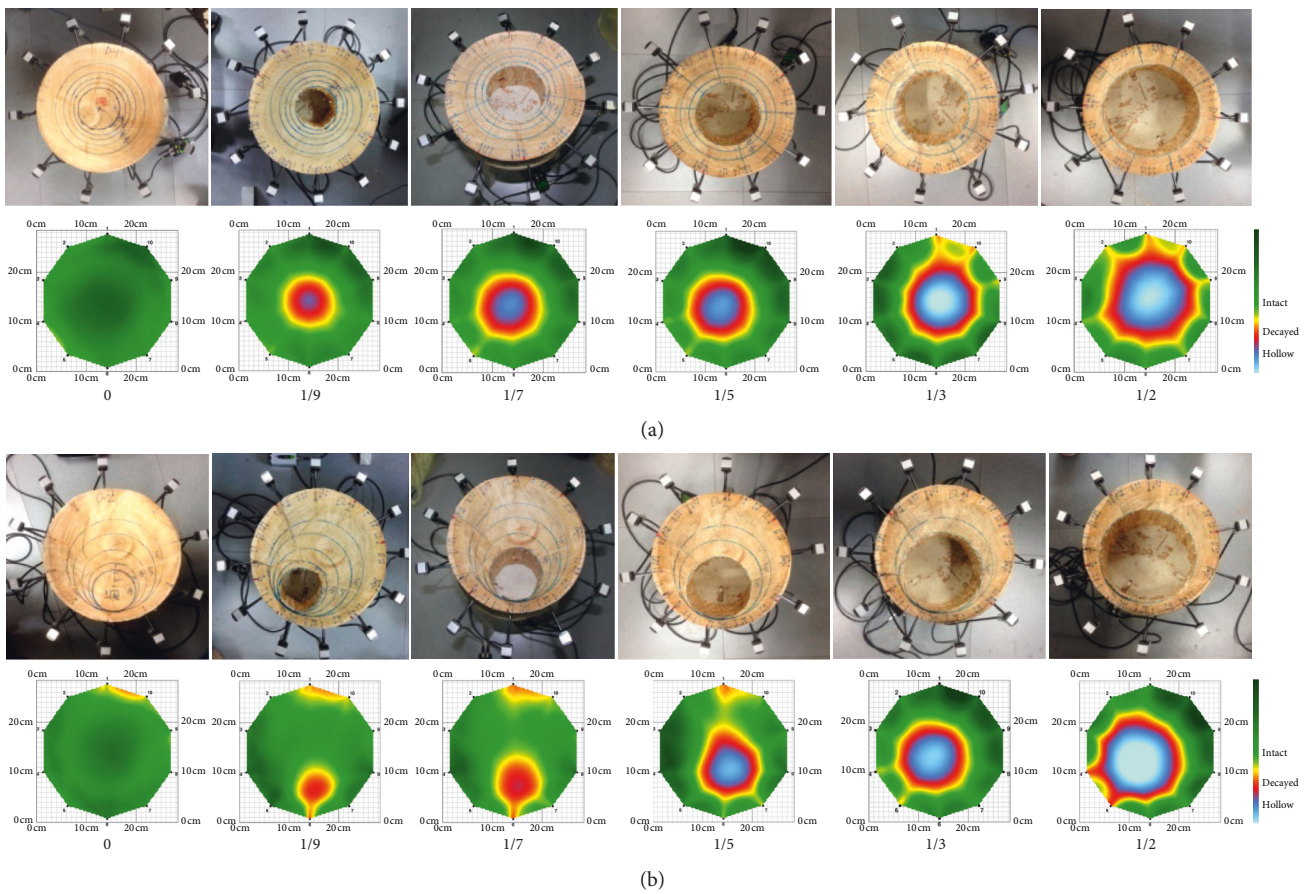

Figure 7: Image of specimens and stress wave diagrams for different stages of defect expansion for (a) the core material cavity experiment and (b) the sapwood cavity experiment.

(any combination of n methods) of I, $E(p)$, $E(q)$ represents the internal defect testing error. The definitions are as follows:

(1) For any subset p, q (any combination of n methods) of I, $E(p) + E(q) \geq E(p \cup q)$

(2) $p \subseteq I$, x_i represents the error value shared when the combination of i method ends, $x_i \leq E(i)$

(3) The overall value $E(n)$ produced by the combined internal defect prediction including n nondestructive

will be completely distributed among n prediction methods, $E(n) = \sum_{i \in n} x_i$

On the assumption that the average method is E_i, the overall error value of the combined prediction is E_i, and

$$E_i = \frac{1}{m} \sum_{j=1}^{m} \left| e_{ij} \right|, \quad (i = 1, 2, \cdots n),$$
$$E = \frac{1}{n} \sum_{i=1}^{n} E_i, \tag{5}$$

where m represents the sample numbers, e_{ij} represents the absolute value of j samples of i nondestructive methods and absolute error of nondestructive testing data.

The weight allocation formula based on the Shapley value algorithm is

$$E_t' = \sum_{p_i \in p} w(|p|)[E(p - \{i\})], \tag{6}$$

$$w|p| = \frac{(n - |p|)!(|p| - 1)!}{n!}, \tag{7}$$

where $w|p|$ is the weighting factor, representing the combined marginal contribution that i should make in combined nondestructive testing; p-$\{i\}$ represents that model i is removed from the combination; i represents a certain nondestructive testing forecasting model involved in the combined prediction; E_i is the error shared by the predicted model i, namely, the Shapley value algorithm; p is any subset of i; and $|p|$ is the number of combined forecasting models.

According to equations (4) and (5), the weight calculation formula of the combined prediction method is as follows:

$$w_i = \frac{1}{n-1} \cdot \frac{E - E_i}{E}, \quad i = 1, 2, \cdots n. \tag{8}$$

5.3. Weight Allocation and Combined Prediction Models of Internal Defects. According to the results of stress wave and impedance meter tests on different defect locations and areas in Table 3, the results of the same specimen show that $S_1 > S_0$ and $S_2 < S_0$. For example, the overall combined prediction error value for specimen D-1 determined by formula (3) is $E = (26.37 + 21.31)/2 = 23.84\,\text{cm}^2$.

In accordance with the concept of the Shapley value algorithm, the member of shared overall values in the combined forecasting model is $I = \{1, 2\}$, whose subset errors are $E\{1\}$, $E\{2\}$, and $E\{1, 2\}$. The numerical values rely on the average values ($26.37\,\text{cm}^2$, $21.31\,\text{cm}^2$, and $23.84\,\text{cm}^2$) of the subset absolute error values.

According to equations (4) and (5), the Shapley value of specimen D-1 stress wave nondestructive testing is

$$\begin{aligned} E_1 &= \frac{1! \times 0!}{2!} [E\{1\} - E(\{1\} - \{1\})] \\ &\quad + \frac{0! \times 1!}{2!} [E\{1, 2\} - E\{1, 2\} - E\{1\}] \\ &= \frac{1}{2}(26.37) + \frac{1}{2}(23.84 - 21.31) = 14.45\,\text{cm}^2. \end{aligned} \tag{9}$$

Similarly, the error shared by specimen D-1 impedance meter nondestructive testing is $E_2 = 9.39\,\text{cm}^2$; this explains that the Shapley value algorithm separately provides weight to each parameter; $E_1 + E_2 = 23.84\,\text{cm}^2$, showing that the sum of the error shared by the individual stress wave and impedance meter testing methods equals the overall error amount E. The shared values reflect the accuracy of each testing method, whose ultimate weight in the combined model depends on equation (6):

$$w_{a1} = \frac{1}{1-1} \cdot \frac{23.84 - 14.45}{23.84} = 0.39, \tag{10}$$

$$w_{a2} = \frac{1}{1-1} \cdot \frac{23.84 - 9.39}{23.84} = 0.61. \tag{11}$$

Similarly, the allocated weights of the nondestructive testing combined model for specimen D-2 are $w_{b1} = 0.45$ and $w_{b2} = 0.55$. According to the above two allocated weights and equation (2), the internal defects of the combined model for specimens D-1 and D-2 are

$$\begin{aligned} f_{D\text{-}1} &= 0.39 \times S_{1(D\text{-}1)} + 0.61 \times S_{2(D\text{-}1)}, \\ f_{D\text{-}2} &= 0.45 \times S_{1(D\text{-}2)} + 0.55 \times S_{2(D\text{-}2)}. \end{aligned} \tag{12}$$

All combined forecasting models are recombined based on their corresponding stress wave and impedance meter testing results to predict internal defect areas. Wooden component internal defect area S_3 is obtained on the basis of the Shapley value combined prediction; the absolute error value, R_3, and relative error value, Q_3, are also obtained (Table 3).

According to Table 3, R_3 is less than R_1 and R_2. To further verify the prediction effect of the combined models on the basis of the Shapley value algorithm, the average relative error values, Q_1 and Q_2, of the stress wave and impedance meter results are calculated. In Table 3, the Q_3 value of specimens D-1 and D-2 combined predicted internal defects is less than that of the individual error values of stress wave or impedance meter results. Moreover, the combined predicted internal defects are more accurate, with an average error value of less than 6%. These results indicate that combined prediction is applicable for detecting internal defect and quantitative analysis of wooden components.

5.4. Combined Prediction and Evaluation of the Wooden Components' Internal Defects. Using Section C and Section D of pillar B2 as examples, we locate internal defects in the sapwood using stress wave two-dimensional plots, which are further confirmed by IML impedance meter tests, indicating that the internal defects are cavities. Internal defects of Section C and Section D are then predicted by hardwood pine and sapwood combined models on the basis of the Shapley value algorithm obtained from reverse laboratory tests. The results indicate that the internal cavity area of Section C is $285.94\,\text{cm}^2$, accounting for 1/3 of Section C, and that of Section D is $249.91\,\text{cm}^2$, accounting for 1/4 of Section D. According to the *Technical Code for Maintenance and Strengthening of Ancient Timber Buildings* [26], compared to the entire section area, the decayed or cavity area in the load-bearing wooden components, P, is greater than 1/5.

Thus, according to our testing data, defects exist in the interior of Section C and Section D of pillar B2 that require renovation.

6. Conclusions

Internal defects within wooden components tend to reduce the compressive area per unit area. Individual nodes or component parts cannot be subjected to normal forces, and then the components of the skew flash or displacement, thereby eventually leading to deformation of ancient building-wood components. In this study, reverse laboratory tests were conducted on major wooden components belonging to the same tree species through nondestructive testing methods. According to defect detection data and experimental results, the following conclusions are drawn:

(1) Internal defects mainly occur in key joints such as pillar bases and girders according to detection tests on wooden components of ancient buildings. Knowledge and analysis of wooden component internal defect characteristics can be used to determine preventive conservation and improve defect detection in ancient architecture.

(2) The sizes and locations of wooden component cavities can be quickly obtained through stress wave tests and effectively visualized using two-dimensional plane detection diagrams. However, stress wave testing area is greater than the actual testing area, errors exist, and internal defect boundaries are blurred.

(3) Using the stress wave results of internal defects in the wood, drilling resistance was used to detect the presence, type, and location of internal defects, which can be accurately confirmed by the corresponding two-dimensional plane detection diagrams. However, the results represent a single path of the testing section and weaker direct detection of internal defects in the entire section. The smaller the internal defects, the more accurate the drilling resistance testing result. The relative error values are directly related to expansion of the defect area. Moreover, more drilling resistance paths may provide more precise information.

(4) The stress wave test chart can determine the approximate position of the internal damage in a wooden component, and the drilling resistance test can determine the shape of the internal damage. The drill resistance test depends on the stress wave test chart, and the drill resistance test results are based on the stress wave test. Therefore, we determined the weight of each prediction method (stress wave and drill resistance tests) using the Shapley value algorithm weight allocation method. This exploits the advantages of both types of nondestructive testing, and using this model, we build an internal defect area prediction model. The predicted result of the combined model based on the Shapley value algorithm is more accurate than that of the single testing method; the internal defect area only exhibits a small prediction error. Through experimental analysis, we determine that the mean relative error of the defect area of the combined prediction model is less than 6%. However, the Shapley value algorithm separately provides weights to each parameter; thus, if one parameter depends on another, different conclusions could be drawn. Therefore, this study presents a new practical method for the quantitative evaluation of internal defects in wooden components, which will be beneficial for architectural heritage conservation as well as provide room for further research.

Data Availability

The data used to support the findings of this study are available from the corresponding author upon request.

Conflicts of Interest

The authors declare that they have no conflicts of interest.

Acknowledgments

This work was supported by the Research Fund for Young Scientists of Da Bei Nong Group (17SK002), the Research Fund for Young Scientists of BUA (SXQN201809), and the National Natural Science Foundation of China (51808038).

References

[1] Y. S. Chen, *The Ancient Wood and Wood Preservation of Cultural Relics*, China Building Industry Press, Beijing, China, 2008.

[2] C. H. Liao, H. J. Zhang, D. Q. Li, and Y. L. Sun, "Development of defect detection methods for ancient architecture components," *Forest Engineering*, vol. 27, no. 4, pp. 51–53, 2011.

[3] T. L. Wang, Y. P. Chen, X. Y. Liu, E. L. Jiang, and R. L. Yu, "Preliminary study on detection of wood structure defects and evaluation of residual elastic modulus," *Journal of Beijing Forestry University*, vol. 32, no. 3, pp. 141–145, 2010.

[4] J. Dai, L. H. Chang, W. Qian et al., "Damage characteristics of ancient architecture wood members and stress wave nondestructive testing of internal void," *Journal of Beijing University of Technology*, vol. 42, no. 2, pp. 236–244, 2016.

[5] Y. Yang and S. J. Shen, "History, present state and future of Non-destructive testing for wood," *Science and Technology Review*, vol. 28, no. 14, pp. 113–117, 2010.

[6] X. Y. Zhang, Y. F. Yin, and X. M. Jiang, "Evaluation of bending properties of Chinese fir plantation by two nondestructive testing methods," *Journal of Building Materials*, vol. 13, no. 6, pp. 836–840, 2010.

[7] S. S. Yu, "Development status of defect detection methods and prospects of ancient wooden buildings," *Forestry Machinery and Woodworking Equipment*, vol. 44, no. 11, pp. 4–13, 2016.

[8] H. J. Zhang, C. Guan, and J. Wen, "Plications and research development of nondestructive," *Journal of Forestry Engineering*, vol. 16, pp. 1–9, 2016.

[9] Y. An, F. Yin, X. M. Jiang, and Y. C. Zhou, "Inspection of decay distribution in wood column by stress wave and resistograph techniques," *Journal of Building Materials*, vol. 11, no. 4, pp. 457–463, 2008.

[10] R. F. Huang, X. H. Wang, H. Li, and X. Y. Liu, "Quantitative analysis on the detected results by resistograph on inside wood decay of architecture," *Journal of Beijing Forestry University*, vol. 29, no. 6, pp. 167–171, 2007.

[11] X. W. Ge, L. H. Wang, Y. T. Sun, Z. X. Liu, J. J. Hou, and Z. Y. Bao, "Quantitative detection of salix matsudana inner decay based on stress wave and resistograph techniques," *China Forestry Science and Technology*, vol. 28, no. 5, pp. 87–91, 2014.

[12] H. Kang and R. E. Booker, "Variation of stress wave velocity with MC and temperature," *Wood Science and Technology*, vol. 36, no. 1, pp. 41–54, 2002.

[13] J. Zhang, N. J. Liao, F. Q. Xu et al., "Research on residual bearing capacity of post-beam timber frame after exposure to fire using non-destructive testing," *China Civil Engineering Journal*, vol. 50, no. 11, pp. 45–56, 2017.

[14] T. N. Liu and L. H. Wang, "Effects of receiving direction angle on amplitude of ultrasonic attenuation tomography on the cross section of logs," *Forest Engineering*, vol. 25, no. 3, pp. 60–65, 2009.

[15] M. P. Wu, *Preventive Conservation of Architectural Heritage in China*, Southeast University Press, Jiangsu, China, 2014.

[16] J. Xiao, J. H. Yang, and N. Huang, "Research of wood intensity supersonic detection system based on DSP," *Forestry Machinery and Wood Working Equipment*, vol. 36, no. 1, pp. 27-28, 2008.

[17] R. J. . Ros, K. A. Mcdonald, L. A. Soltis et al., "NDE of historical structures -USS constitution," in *Proceedings of Nondestructive Evaluation of Materials and Composites, SPIE 2944*, pp. 266–274, November 1996.

[18] F. Divos, L. Nemeth, and L. Bejo, "Evaluation of the wooden structures of a Baroque palace in Papa, Hungary," in *Proceedings of the 11th International Symposium on Nondestructive Testing of Wood*, Sopron, Hungary, May 2005.

[19] J. Zhang, Q.-f. Xu, Y.-x. Xu, and M. Zhang, "Research on residual bending capacities of used wood members based on the correlation between non-destructive testing results and the mechanical properties of wood," *Journal of Zhejiang University-SCIENCE A*, vol. 16, pp. 541–550, 2015.

[20] X. Q. Yue, L. H. Wang, X. L. Wang et al., "Quantitative detection of internal decay degree for standing trees based on three NDT methods—electric resistance tomography," *Scientia Silvae Sinicae*, vol. 53, no. 3, pp. 139–145, 2017.

[21] X. L. Shi, L. H. Wang, H. D. Xu et al., "Quantitative characterization of decay detection in standing trees of Korean pine based on Resistograph and ERT," *Journal of Beijing Forestry University*, vol. 39, no. 9, pp. 102–111, 2017.

[22] X. M. Jiang, Y. M. Cheng, Y. F. Yin et al., *Chinese Gymnosperms*, Science Press, Beijing, China, 2010.

[23] X. Q. Deng, W. Z. Li, J. G. Wu et al., "Hybrid feature selection algorithm fused Shapley value and particle swarm optimization," *Journal of Computer Applications*, vol. 38, no. 5, pp. 1245–1249, 2018.

[24] X. P. Lei, Q. Robin, X. Lei, Q. Robin et al., "Research on improvement and application of Shapley value," *Computer Engineering and Applications*, vol. 48, no. 7, pp. 23–29, 2012.

[25] C. Liu, L. Song, and J. T. Meng, "Interval-valued fuzzy Shapley value for risk sharing of PPP model for water diversion project," *Water Resources and Power*, vol. 36, no. 6, pp. 162–166, 2018.

[26] GB 50165-92, *Technical Code for Maintenance and Strengthening of Ancient Timber Buildings*, National Standard of the People's Republic of China, China, 1992.